

Accepted Article

Development of a Hybrid Shrinking-Core Shrinking-Particle Model for Entrained-Flow Gasifiers

This is the author manuscript accepted for publication and has undergone full peer review but has not been through the copyediting, typesetting, pagination and proofreading process, which may lead to differences between this version and the [Version record](#). Please cite this article as [doi:10.1002/aic.15055](https://doi.org/10.1002/aic.15055).

Development of a Hybrid Shrinking-Core Shrinking-Particle Model for Entrained-Flow Gasifiers

Pratik Pednekar¹, Debangsu Bhattacharyya^{1,*}, Job S. Kasule¹, Richard Turton¹,
and Raghunathan Rengaswamy²

¹Department of Chemical Engineering, West Virginia University, Morgantown, WV 26506

²Department of Chemical Engineering, Texas Tech University, Lubbock, TX 79409

Abstract

The slagging entrained-flow gasifiers operate above the melting temperature of the ash. Since slag is highly non-wetting on the surface of char (carbon) particles, it is likely that it will agglomerate into one or several slag droplets and some of these droplets can detach from the char particles. If the slag exists in the form of droplets on the char surface rather than as a solid shell around the unreacted char particle, a shrinking particle model (SPM) would be more physically realistic representation in comparison to the widely-used shrinking core model (SCM). In the early section of the gasifier, the temperature remains below the ash melting temperature and therefore, the SCM is more appropriate in this region. With this motivation, a novel hybrid shrinking-core shrinking-particle (HSCSP) model has been developed. The model provides spatial profile of a number of important variables that are not available from the traditional SCM.

Keywords: entrained-flow, gasifier, shrinking particle model, shrinking core model, slag

*Corresponding author. Tel: +1-3042939335, Fax: +1-3042934139

E-mail address: Debangsu.Bhattacharyya@mail.wvu.edu

Introduction

Entrained-flow gasifiers operate at very high temperatures to provide high carbon conversion¹. At these high temperatures, gasifiers operate under slagging condition, i.e., the ash melts to form a liquid slag. A portion of the slag flows down the refractory wall. The slag can penetrate into the wall and can cause degradation of the refractory at an accelerated rate²⁻³. Refractory degradation is one of the leading issues that impact economic viability of the entrained-flow gasifiers⁴.

A number of papers have investigated the flow of slag on the gasifier wall⁵⁻⁹. All these papers have considered that a fraction of the char particles hits the flowing slag layer on the wall of the gasifier. A fraction of these char particles sticks to the wall and continues to react. As a result, the ash contained in these char particles melts contributing to the slag layer. Since it is assumed that the ash remains attached to the reacting char particles in the bulk of the gasifier, a shrinking core model is considered to describe the kinetics^{6, 8, 10, 11}. In the shrinking core model, the ash contained in the char particles is assumed to form a solid shell around the unreacted carbon core. The overall size of the char particle remains unchanged while its density decreases as the core shrinks.

However, due to the very high operating temperature of the entrained-flow gasifiers, it is expected that the ash gets molten in such environments as suggested by a number of researchers¹²⁻¹⁴. There are several papers that have reported that for combustion systems, liquid slag does exist as droplets in the bulk¹⁵⁻¹⁸. Depending upon the composition of the ash content in coal, the melting points of ash can vary greatly. Ash from the Illinois #6, Pittsburgh #8, and PRB coals for most of the seams is expected to have a melting temperature lower than 1350°C¹⁹. The exit temperature from the entrained flow gasifiers is typically 1350-1600°C. The temperature immediately after the devolatilization section in which the combustion reactions take place, often

exceed the outlet temperatures by a few hundred degrees. Therefore, for a major section of the gasifier, the temperature would exceed the melting point of the ash in an entrained flow gasifier.

Since slag is highly non-wetting on the surface of carbon²⁰⁻²¹ when the ash melts, it is likely that it will agglomerate into one or several slag droplets rather than spread over the surface of the char particle. Several papers²²⁻²⁴ in the literature have shown, using SEM, the existence of liquid slag droplets on the char surface but there is hardly any work that has modeled this phenomenon.

If the slag exists in the form of droplets on the char surface rather than as a solid shell around the unreacted char particle, then the widely-used shrinking core model (SCM) does not seem physically correct. Rather, a shrinking particle model (SPM) would be more physically realistic representation. Unlike the shrinking-core model that assumes the diameter of the char particle to be constant²⁵, the shrinking-particle model considers the char particle to shrink while the slag droplet(s) would build up on the particle's surface. Eventually the slag droplets may detach from the char surface moving into the gasifier bulk. More included mineral matter gets exposed on the surface leading to the formation of new droplets. This suggested mechanism is shown in Figure 1.

Very few papers in the area of modeling look into the process of slag detachment. The dominant mechanism for the addition of ash to the slag flow layer on the refractory is assumed to be due to the impaction of char particles. A few papers do point out that slag droplets also get deposited on the slag flow layer; however, clarity on how these slag droplets exist in the gasifier bulk is lacking.

A size distribution of slag droplets is found to exist in the bulk^{16, 23-27}. The size distribution is often a strong function of the conditions, coal sizes and coal types. It could range from sizes

greater than 30 microns to submicron²⁸. Smaller, submicron slag droplets are formed predominantly due to vaporization and consequent condensation of metal oxides²⁹. Larger slag droplets are formed as a result of complete coalescence. In this scenario, all the mineral content in the char particle coalesce to form a single slag droplet²⁷⁻²⁸. Given the extreme conditions within the gasifier, it is not necessary that the agglomerated mineral matter will only detach from the char particle when it approaches complete burnout. It is found that the separation of individual included mineral matter or partially coalesced mineral inclusion is found to result in sizes between 1-20 microns due to shedding or char fragmentation²⁴. At higher temperature operations, it has been shown that the amount of PM-10 slag droplets is high and this is attributed to the shedding of included minerals from fast receding surface²⁴. The dominant mass fraction of the ash in the bulk is accounted for by complete coalescence and PM-10 particles. In this study, therefore, these two methods of slag droplet formation in the bulk are examined individually.

From the previous discussion, a shrinking-particle model seems more physically correct for the region where the gasifier bulk temperature well exceeds the ash melting temperature. However, in the early region of the gasifier, where the bulk temperature remains lower than the ash melting temperature, a shrinking-core model seems more appropriate. Therefore, in this work, we have developed a novel first principles, one-dimensional, non-isothermal, pressure-driven dynamic model for a downward-firing, entrained-flow, slurry-fed, oxygen-blown (GEE-Texaco type) gasifier using a hybrid shrinking-core-shrinking-particle reaction model. The developed model is then used to study the effects of various key variables on the slagging process and compare them with the results for the traditional shrinking-core models. Complete coalescence and slag detachment scenarios are simulated and the impact on slag build-up on the char surface and slag

droplet number density in the gasifier bulk is studied. To the best of the authors' knowledge, this is the first attempt to quantify the amount of detached slag droplets present in the entrained-flow gasifiers. The detached slag droplets can result in additional contribution to the slag layer in addition to the contribution by the char particles. As the thickness of the slag layer is one of the key operating variables, yet unmeasurable so far, this model can be enhanced for estimating slag layer thickness under different operating conditions.

Model

Background and description

The shrinking-core model used in this work has been previously presented by Kasule^{10, 31} et al. and is used for the early region of the gasifier where the bulk temperature is below the ash melting temperature. Details of that model can be found in the work of Kasule et al. It should be noted that in entrained-flow gasifiers, burners are designed to promote swirling motion at the top of the gasifier that results in quick evaporation of water and the subsequent devolatilization step followed by combustion of the liberated volatile matter leading to a significant temperature peak. The high carbon residue formed after these processes is called char. From that region to the exit of the gasifier, the solids temperature remains well above the melting point of ash. Therefore the shrinking particle model is applied to that region. Figure 2 shows the regions where shrinking core and shrinking particle models are applied.

The shrinking particle model presented below is novel and to the best of the knowledge of the authors, has never been proposed for the gasifier. The shrinking particle model is one-dimensional and considers both the solid and gas phases. Mass, momentum and energy equations are written for both phases. The molten slag in the bulk as well as attached to the char particle is considered to be part of the solid phase. The dimensions of the gasifier are based on the GEE-

Texaco gasifier³⁰. A rigorous model for the heat balance on the gasifier wall is also considered. Gas recirculation is also modelled, similar to the shrinking core model^{10,31}, to mimic the swirling effect produced by the burners.

The entrained flow gasifier is intended to be used as a process models in order to perform dynamic simulations and control studies. Therefore, it is required to be rigorous at the same time computationally tractable. In order to do so, the following assumptions have been made in developing the shrinking-particle model:

1. Char particles and slag droplets are spherical.
2. Radial distribution of char particles is uniform.
3. Slag separation occurs uniformly for all char particles.
4. No particle-particle interaction; system is assumed to be sparse.
5. No slag deposition is considered in the present work.
6. Three discrete detachment diameters are used in this work. These are 5, 10 and 15 μm . A complete coalescence case is also considered.
7. The velocities of the char particles and detached slag droplets are assumed to be equal. This assumption results in a single momentum balance equation aiding to the desired computational efficiency of this dynamic model that is intended to be used for dynamic and control studies. The rationale behind this assumption is very dilute condition prevalent in the entrained-flow gasifiers and the small sizes of the solids present in the process. In entrained flow gasifiers, the volume fraction of solids is less than 1%¹¹. In addition, the coal particle sizes at the inlet are lesser than 100 micron in diameter and for such systems, the differences between gas and solid velocities are found to be negligible even while considering the traditional shrinking core model³². As the size of the detached slag droplets and the char

particles in the shrinking particle model would be smaller than the char particles in the shrinking core model, their velocity would also be expected to be close to the gas velocity.

Therefore, the assumption that the char particles and detached slag droplets have similar velocities seems reasonable.

Both the solid and gas phases are modeled as continuous phases. A particle model is developed to account for the slag droplets that are attached to the char particles and for the detached slag droplets that exist in the bulk and is integrated with the continuous phase model. A few notations need to be described before presenting the model. The gas phase volume fraction is denoted as ε . The solid phase, with volume fraction $(1-\varepsilon)$, is divided into the volume fraction of the slag droplets in the bulk, given by ε_{sd} and the volume fraction of the char-slag system, i.e., char particles with the slag droplets attached to them and is denoted as $(1-\varepsilon_{sd})$. The attached slag droplet to the char particles is accounted for by the volume fraction ε_{sa} . The notations are shown in Figure 3.

Continuous phase model

The continuous phase model is developed for the gas phase and overall solid phase. Additional conservation equations are written for slag droplets that are attached to the char particles as well as for the slag droplets that are detached.

Mass conservation equations

Eq. 1 shows the overall solid phase mass conservation. In this equation, the second term on the right hand side represents the solids loss due to reaction where the reaction rate has been defined with respect to the char particle. As seen in Figure 3, the volume fraction corresponding to the char particle is $(1-\varepsilon)(1-\varepsilon_{sa})(1-\varepsilon_{sd})$. The solids can also be lost from the bulk due to

deposition on the gasifier wall as given by the third term in Eq. 1. Eq. 2 shows the gas phase mass conservation equations.

$$\frac{\partial(\rho_{s,avg}(1-\varepsilon))}{\partial t} = -\frac{\partial(\rho_{s,avg}(1-\varepsilon)U_s)}{\partial x} - (1-\varepsilon)(1-\varepsilon_{sa})(1-\varepsilon_{sd})\Gamma_{s-g} - \frac{4M_{slag\ dep.}}{D_i} \quad (1)$$

$$\frac{\partial(\rho_g\varepsilon)}{\partial t} = -\frac{\partial(\rho_g\varepsilon U_g)}{\partial x} + (1-\varepsilon)(1-\varepsilon_{sa})(1-\varepsilon_{sd})\Gamma_{s-g} - m_{rg} + m_{mg} \quad (2)$$

In Eqs. 1 and 2, $\rho_{s,avg}$ and ρ_g are the average solid and gas densities, U_s and U_g are the solid and gas velocities, Γ_{s-g} is the sum of all heterogeneous reactions, $M_{slag\ dep.}$ is the mass deposition rate of slag onto the gasifier wall in the control volume and D_i is the internal wall diameter. In this work, the deposition of char onto the gasifier wall is not considered.

The recirculation effect in the gas phase is captured by the terms m_{rg} , which is the mass of gas that leaves the control volume (CV) because of recirculation, and m_{mg} , which is the mass of gas that gets added to a CV due to recirculation. These terms are calculated by the following equations:

$$m_{rg} = \dot{m}_{recir}/A_R L_2 \quad (3)$$

$$m_{mg} = \dot{m}_{recir}/A_R L_1 \quad (4)$$

$$\dot{m}_{recir} = \alpha \dot{m}_{in} \quad (5)$$

where A is the cross section area, L_2 is the length of the zone from where the recirculating gas is removed and L_1 is the length of the zone where the gas is added into the bulk gas stream, α is the recirculation ratio and \dot{m}_{in} is the inlet gas stream. A schematic of the recirculation model is shown in Figure 4.

Eqs. 3 and 4 show the species conservation equations for the solid and gas phases, respectively.

$$\frac{\partial((1-\varepsilon)(1-\varepsilon_{sa})(1-\varepsilon_{sd})\rho_{ch}X_{s,j})}{\partial t} = -\frac{\partial((1-\varepsilon)(1-\varepsilon_{sa})(1-\varepsilon_{sd})\rho_{ch}U_sX_{s,j})}{\partial x} + (1-\varepsilon)(1-\varepsilon_{sa})(1-\varepsilon_{sd})r_{s,j} \quad (6)$$

$$\frac{\partial(\varepsilon\rho_g y_{g,i})}{\partial t} = -\frac{\partial(\varepsilon\rho_g U_g y_{g,i})}{\partial x} + \varepsilon r_{g,i} - m_{rg}y_{g,i} + m_{mg}y_{g,i,avg} \quad (7)$$

The volume fraction corresponding to the char particle volume, shown in Figure 4 is used in Eq. 6 for each of the terms. The last two terms in Eq. 7 correspond to the recirculation of gas species out of and into the control volume similar to the overall gas balance equation. $y_{g,i}$ is the mass fraction of the species i . $y_{g,i,avg}$ denotes the average mass fraction of species i in the circulating flow. Details of the recirculation model can be found in the work of Kasule et al¹⁰.

The gas phase density is calculated by assuming ideal gas law in the form given by Eq. 8.

$$\rho_g = \frac{P}{RT_g} \cdot \frac{1}{\sum_{i=1}^N (y_i/MW_i)} \quad (8)$$

In Eq. 8, N is the total number of gaseous species and y_i and MW_i are the mass fraction and molar weight of the i^{th} gaseous species.

Mass conservation of attached slag

Eq. 9 represents the mass conservation of attached slag.

$$\rho_{sl} \frac{\partial((1-\varepsilon)(1-\varepsilon_{sd})\varepsilon_{sa})}{\partial t} = -\rho_{sl} \frac{\partial((1-\varepsilon)(1-\varepsilon_{sd})\varepsilon_{sa}U_s)}{\partial x} + (1-\varepsilon)(1-\varepsilon_{sa})(1-\varepsilon_{sd})\Gamma_{s-g}\omega_{ash} - p_{sl}M_{cd} \quad (9)$$

Mass is added to the attached slag droplet as ash melts during heterogeneous reactions as represented by the second term on the right hand side. The third term accounts for separation of the slag droplet into the bulk, where, p_{sl} denotes number of slag droplets separated per unit volume per unit time and M_{cd} is the mass of the slag droplet of the critical diameter. It is noted that, p_{sl} will be zero for a CV if no slag detachment has taken place in that CV.

Mass conservation of detached slag

As mentioned before, it has been assumed that as the slag droplet size exceeds some critical diameter, it gets detached from the char particle. Therefore, the slag separation is not a continuous process. With this assumption, the mass conservation equation for detached slag droplets is given as Eq. 10.

$$\rho_{sl} \frac{\partial((1-\varepsilon)\varepsilon_{sd})}{\partial t} = -\rho_{sl} \frac{\partial((1-\varepsilon)\varepsilon_{sd}U_s)}{\partial x} + p_{sl}M_{cd} - \frac{4*M_{slag\ dep.}}{D_i} \quad (10)$$

Particle model

For the continuous model, it is important to know the magnitude of the terms p_{sl} as well as the amount of slag that gets deposited on the wall. In this work, it has been assumed that the amount of slag deposited on the wall is zero, i.e. all slag exits through the bulk of the gasifier in order to make an unbiased comparison of results from the traditional shrinking-core model. However, for calculating the term p_{sl} , a particle model is required. This model tracks the growth of the slag droplets on the char particle and helps to identify the locations of detachment and the detachment rate. Then this model is used to track the number density of slag droplets and char particles in the gasifier bulk.

Figure 5 shows that on an overall scale, a continuum description is used for the gas and solid mass balance. In order to account for the number of slag droplets, a particle phase model is used under the continuum description such that the overall mass balance of the continuum is still satisfied.

Slag detachment model

The slag detachment is not a continuous process as pointed out. Therefore, algebraic equations are developed to model this process. Figure 6 shows the schematic of the slag formation and detachment model. The term p_{sl} is calculated from Eq. 11:

$$p_{sl,i}\tau_i = w_{sl,i}N_{ch,i} \quad (11)$$

$$\tau_i = \frac{\Delta x}{U_{s,i}} \quad (12)$$

In Eq. 12, τ_i is the residence time of the solids in the i^{th} control volume (CV); $w_{sl,i}$ is the number of slag droplets generated per char particle in the CV; and $N_{ch,i}$ is the number of char particles per unit volume in the CV. The term $w_{sl,i}$ is calculated from Eq. 11.

$$w_{sl,i} = \text{floor} \left(\frac{\omega_{ash}\Gamma_{s-g,i}V_{ch,i}\tau_i + M_{sr,i-1}}{M_{cd}} \right) \quad (13)$$

where, ω_{ash} is the ratio of ash to carbon mass fraction. As can be seen, until the attached slag mass exceeds the critical slag mass, the value of $w_{sl,i}$ is zero. It is possible that if the critical mass is small or the reaction rate is very high, multiple slag droplets can form in a single control volume.

It should also be noted that in the shrinking-particle model, the mass fraction of the ash and carbon in the char remain unchanged due to assumption of homogeneous composition.

Therefore, the ω_{ash} term is constant. $V_{ch,i}$ is the volume of the char particle in the CV. $M_{sr,i-1}$ denotes the residual mass of the slag droplet from the previous control volume. The residual mass of the slag droplets accounts for the mass of the slag droplets attached to the char particles from previous CVs. It should be noted that this term captures the mass of the slag droplets that did not get separated. Finally M_{cd} is the critical mass of the slag droplet.

The slag droplet formation is described by Eq. 14, where $M_{sr,i}$, which is the amount of slag left behind after separation of the slag droplet.

$$w_{sl,i}V_{cd}\rho_{sl,i} + M_{sr,i} = \omega_{ash}\Gamma_{s-g,i}V_{ch,i}\tau_i + M_{sr,i-1} \quad (14)$$

The first term on the left hand side of Eq. (14) is the amount of slag that became separated in the i^{th} CV. The first term on the right hand side represents the amount of slag generated in the i^{th} CV.

This can be better understood from the top of Figure 5.

The char particle mass balance equation is given by Eq. 15.

$$M_{ch,i} = M_{ch,i-1} - \Gamma_{s-g,i}V_{ch,i}\tau_i(1 + \omega_{ash}) \quad (15)$$

The second term on the right hand side of Eq. 15 includes the loss of mass from the char particle due to heterogeneous reactions and due to slag formation. The heterogeneous reactions determine the rate at which the size of the char particle shrinks. The volume of the char particles is calculated from Eq. 16.

$$M_{ch,i} = V_{ch,i}\rho_{ch} \quad (16)$$

The density of the char particle, ρ_{ch} , in the slagging section of the gasifier is constant since a shrinking particle model is assumed. The density of the char particle is calculated by excluding moisture and volatile matter²⁵.

The overall mass balance for the char particles using both continuous and particle descriptions must be the same, as given by Eq. 17.

$$N_{ch,i}V_{ch,i} = (1 - \varepsilon_i)(1 - \varepsilon_{sa,i})(1 - \varepsilon_{sd,i}) \quad (17)$$

where, $V_{ch,i}$ represents the volume of a single char particle in the i^{th} CV.

Figure 7 shows how the continuum model is coupled with the particle model. The coupling is done by number averaging with the assumption that the char particles are homogeneous in composition and equal in size in the same control volume. $w_{sl,i}$ as defined in Eq. (13) is an integer variable and therefore, a number averaged variable $p_{sl,i}$ is calculated from it using Eq. (11) and used in Eq. (9) and (10) for the continuum model. In addition, the volume fractions used in the continuum model are related to the particle model by Eq. (17).

Momentum balance equation

As mentioned earlier the velocities of the slag droplets, both attached and detached, are assumed to be the same as the char particles. Under this assumption, momentum balances are required only for the gas phase and the overall solid phase and these balances are shown in Eqs. 18 and 19, respectively.

$$\frac{d(\varepsilon\rho_g U_g^2)}{dx} = -\varepsilon \frac{dP_t}{dx} + \varepsilon\rho_g g - (1 - \varepsilon)f_s \quad (18)$$

$$\frac{d((1-\varepsilon)\rho_{s,avg} U_s^2)}{dx} = -(1 - \varepsilon) \frac{dP_t}{dx} + (1 - \varepsilon)\rho_{s,avg} g + (1 - \varepsilon)f_s \quad (19)$$

where, f_s is the drag force per unit volume of particles, U_s and U_g are the solid and gas phase velocities respectively, P_t is the total pressure in the system. The drag force is calculated using the equation from Arastropour and Gidaspow³³ as;

$$f_s = \frac{3C_D\rho_g(1-\varepsilon)^{-2.65}(U_g-U_s)|U_g-U_s|}{4d_{avg}} \quad (20)$$

where the C_D is the drag coefficient taken from Rowe and Henwood³⁴. This is given as

$$C_D = \begin{cases} \frac{24}{Re} [1 + 0.15Re^{0.687}] ; Re < 1000 \\ 0.44 ; Re \geq 1000 \end{cases} \quad (21)$$

The Reynolds number is given as

$$Re = (1 - \varepsilon)\rho_g d_{avg} \frac{|U_g - U_s|}{\mu_g} \quad (22)$$

where, μ_g , is the viscosity of the gas phase and d_{avg} is the weighted average diameter of the slag droplets and char particles, calculated on the basis of their respective volume fractions.

Energy balance equation

The energy balance equations for the gas and solid phases are shown in Eqs. 23 and 24. The temperature of the slag droplets and the char particle are assumed to be equal. This is done mainly for simplicity and keeping the computational expense tractable for a dynamic model. The model can be easily enhanced by relaxing this assumption.

$$\frac{\partial(\varepsilon\rho_g C_{p,g} T_g)}{\partial t} + \frac{\partial(U_g \varepsilon \rho_g C_{p,g} T_g)}{\partial x} = \frac{\pi D_i}{A_R} \{h_{w-g} [T_w - T_g]\} - (1 - \varepsilon) \frac{6}{d_{char}} \{e_g F_{g-s} \sigma [T_g^4 - T_s^4] + h_{g-s} [T_g - T_s]\} + \sum_j^{gas-phase} \varepsilon (-\Delta H_{rxn,j}) r_j - m_{rg} h_{rg} + m_{mg} h_{mg} \quad (23)$$

$$\frac{\partial((1-\varepsilon)\rho_{s,avg}C_{p,avg}T_s)}{\partial t} + \frac{\partial(U_s(1-\varepsilon)\rho_{s,avg}C_{p,avg}T_s)}{\partial x} = \frac{\pi D_i}{A_R} F_{w-s} [T_w^4 - T_s^4] + (1 - \varepsilon) \frac{6}{d_{char}} (e_g F_{g-s} \sigma [T_g^4 - T_s^4] + h_{g-s} [T_g - T_s]) + \sum_k^{solid-phase\ reactions} (1 - \varepsilon) (-\Delta H_{rxn,k}) r_k \quad (24)$$

where F_{g-s} and F_{w-s} are the view factors between gas-solid and wall- solid, respectively. In the gas phase energy balance equation, $m_{rg}h_{rg}$ is the enthalpy leaving and $m_{mg}h_{mg}$ is the enthalpy entering the control volume due to recirculation. $\Delta H_{rxn,j}$ and $\Delta H_{rxn,k}$ are the heat of reaction for the homogeneous and heterogeneous reactions, respectively. The heat of reactions and kinetic parameters have been taken from the literature cited in Kasule et al¹⁰. The authors could not find the heat of fusion for the ash in Illinois #6 coal, however, based on the limited literature, it seems that the heat of fusion for ash in coal^{35,36} is usually very small in comparison to the heat of reaction of the heterogeneous reactions. Therefore, the heat of fusion is not explicitly considered in this model. Furthermore, ash transformation reactions are not considered separately, but are assumed to take place spontaneously along with the char conversion reactions. Due to this assumption, the latent heat of fusion for ash can be readily included in the energy balance equations by modifying the heat of reaction for the heterogeneous reactions. In the solid phase energy balance equation, $C_{p,avg}$ is the average specific heat calculated using the weighted average of the voidage fractions of char, slag droplets attached and slag droplets in the bulk. Eqs. 25-26 show how h_{rg} and h_{mg} are calculated.

$$h_{rg} = \sum_{i=1}^N y_i \int_{298}^T C_{p,i} dT \quad (25)$$

$$h_{mg} = \frac{1}{m} \sum_{k=1}^r h_{rg,k} \quad (26)$$

where N is the number of components in the gas phase, r is the number of control volumes in the recirculation zone and m is the number of control volumes in the mixing zone.

Eqs. 27-29 are used for the calculation of the average density and specific heat that is used in the momentum and energy balance equation for the solid phase.

$$\rho_{s,avg} = \varepsilon_{sd}\rho_{sl} + (1 - \varepsilon_{sd})\varepsilon_{sa}\rho_{sl} + (1 - \varepsilon_{sd})(1 - \varepsilon_{sa})\rho_{ch} \quad (27)$$

$$d_{avg} = \varepsilon_{sd}d_{cr} + (1 - \varepsilon_{sd})\varepsilon_{sa}d_{sa} + (1 - \varepsilon_{sd})(1 - \varepsilon_{sa})d_{ch} \quad (28)$$

$$\rho_{s,avg}C_{p,avg} = \varepsilon_{sd}\rho_{sl}C_{p,slag} + (1 - \varepsilon_{sd})\varepsilon_{sa}\rho_{sl}C_{p,slag} + (1 - \varepsilon_{sd})(1 - \varepsilon_{sa})\rho_{ch}C_{p,ch} \quad (29)$$

The wall energy balance is taken from Kasule¹⁰ et al., and includes radiation between the wall and solids, radiation between wall and the top and bottom of the gasifier respectively, convection between wall and gas and the energy loss to the surrounding environment.

$$\rho_{wall}C_{p,wall} \frac{(D_o^2 - D_i^2)}{4} \frac{d(T_w)}{dx} = (\pi D_i \Delta x) \sum_i (q_{conv,w-g} + q_{rad,w-g} + q_{cond,w-skin} + q_{rad,w_i - q_{all,p \neq i}} + q_{rad,w-top} + q_{rad,w-btm}) \quad (30)$$

where,

$$q_{conv,w-g} = h_{w-g}(T_w - T_g)$$

$$q_{cond,w-skin} = k_{eff,w} \frac{(T_w - T_{skin})}{((D_o^2 - D_i^2)/4)}$$

$$q_{rad,w-s} = F_{w-s}\sigma(T_w^4 - T_s^4)$$

$$q_{rad,w_i - w_{all p \neq i}} = \sum_p e_w F_{w_i - w_p} (T_{w_i}^4 - T_{w_p}^4)$$

Reaction rates

The gasifier can be divided into several reaction zones based on the dominant reactions/processes that occur in the solids. These reactions/ processes include drying, devolatilization, combustion, and gasification. The first three of these processes tend to occur

much earlier in the gasifier, and result in a dramatic increase in the solid temperature. Gasification reactions are slower and continue till the end of the gasifier. In both shrinking core and shrinking particle models, all reactions are considered at all locations.

Water vapor evaporation, devolatilization and the homogeneous reactions are modeled in the same manner as shown in Kasule et al.¹⁰. Water evaporation is modeled similar to the work of Rao et al.³⁷ A point to note is that the water in the slurry and the moisture content is considered together in calculation of the evaporation rate. For devolatilization, the products and kinetic parameters for the reaction / processes given by Syamlal and Bisset³⁸ are used in the model.

The overall reaction rate for the shrinking core model is given by:

$$K_{overall} = \frac{1}{\frac{1}{k_{diff}} + \frac{1}{k_{ash}} \left(1 - \frac{1}{Y}\right) + \frac{1}{k_s Y^2}} \quad (31)$$

where Y is the ratio of the diameters of unreacted core and the char particle, and k_{diff} , k_{ash} and k_s are the gas film diffusion coefficient, ash diffusion coefficient and surface reaction coefficient respectively.

In contrast to the shrinking-core model, the shrinking particle model considers no resistance due to ash. The overall rate constant for a shrinking particle model is given by:

$$K_{overall} = \frac{1}{\frac{1}{k_{diff}} + \frac{1}{k_s}} \quad (32)$$

It can be noted that all rate constants are in the units of $\text{g}\cdot\text{cm}^{-2}\cdot\text{atm}^{-1}\cdot\text{s}^{-1}$. The expressions for the coefficients are taken from the work of Wen and Chaung³⁹. Typically, a conversion factor of $6/d_{char}$ is used to give the overall reaction rate constant in terms of volumetric units. For the present model, the surface reaction rate constant term cannot be evaluated at a shrinking particle

size since the reaction rate would tend to infinity as the diameter of the char particle shrinks to zero. The surface reaction rate constant is instead converted to volumetric units by evaluating the factor $6/d_{char}$ at the fixed char particle size. The particle size used by Wen and Chaung³⁹ had considered while developing these kinetics was 350 μ m.

Model inputs

The model for the slagging gasifier has been developed in Aspen Custom Modeler[®] (ACM⁴⁰). The system of partial differential equations and algebraic (PDAE system) are solved simultaneously using a backward finite difference method. Table 1 lists model parameters and input conditions.

Results and Discussions

The results from the HSCSP model are summarized below. These include the validation of the data as compared to the TECO power plant⁴¹, comparison with the traditional shrinking-core model, profiles of key variables and a sensitivity analysis on the detachment diameter.

Model Validation

In this section, the results were obtained assuming complete coalescence of slag droplets, which should closely resemble the results from the shrinking-core model assuming no slag detachment. This is compared first with the industrial data of TECO power plant⁴¹. The gasifier configuration of the TECO power plant and the operating conditions are shown in Table 3.

The data from the TECO power plant are available for the clean syngas that is downstream of the radiant syngas cooler (RSC). In the RSC, steam is produced by utilizing the energy in the gasifier exit stream. It has been reported that certain gas-phase reactions, such as the water-gas shift

reaction, continue to take place in the initial section of the RSC¹⁰. Therefore, for comparing the results with the TECO Power plant, a simple model of the RSC was developed in Aspen Plus.

The RSC is modeled using a plug flow reactor. This model is implemented in a similar manner as done in the work of Kasule¹⁰. A constant cooler temperature of 609 K was assumed.

Figure 8 shows that the results from the HSCSP model shows a good qualitative agreement with the TECO data.

Shrinking core vs HSCSP model

The results from this work are compared with the shrinking-core model developed by Kasule et al.¹⁰ For a fair comparison, feed composition, flow rates, pressures, and O₂/Coal ratio are set to be the same in both the models.

Figure 9 shows the heterogeneous reaction rates for both the models after combustion of char takes place, i.e., in the region where the SPM is applied. In the SCM, the overall reaction rate is limited by the resistance due to the ash layer which is zero for the SPM model. Furthermore, the diffusion resistance of a shrinking particle would be lower than that calculated in the SCM. However, the volume of the particle keeps decreasing in the SPM. Overall, there is hardly any difference in the heterogeneous reaction rate as shown in Figure 9.

Figure 10 compares carbon conversion obtained in this work to that obtained using the SCM. In both the cases, a significant amount of carbon gets converted very early in the reactor followed by slower conversion, which is mainly due to the gasification reactions.

Figure 11 compares the temperature of the char particle using the SCM with the HSCSP model developed in this work. As mentioned earlier, in the initial region of the gasifier up to the point

when the bulk temperature exceeds the ash melting temperature the HSCSP model considers shrinking core assumption and therefore, the solid and gas temperatures closely match that from the SCM in this region. Therefore in Figure 11, the solids temperature profile beyond this initial region is compared. The solids temperature from the HSCSP model is found to be little higher towards the beginning of this section. However, towards the end, both models reach similar conversion and the exit temperatures are the same. The gas temperature also follows the same trend (not shown here).

Comparing the mole fractions at the exit of the gasifier for the SCM and HSCSP models in Table 4, we see that there is very little difference between the two models.

Complete coalescence scenario

In this scenario, it is assumed that the slag droplets are not detached from the char particles. Figure 12 shows that even though the char conversion is high, the char particle still exits at some finite size that exits the gasifier. The slag droplet attached to the char particle grows rapidly initially when the conversion is high. It begins to level off towards the end due to the decrease in conversion rate.

Figure 12 shows the profiles for the diameters and densities in the zone where the SPM is applied, i.e., after the bulk temperature increases beyond the ash melting temperature. Figure 12 also shows that the average density calculated using Eq. 27 keeps increasing along the gasifier as char content continues to decrease while slag content keeps increasing, which is because the slag droplets have higher density than the char particles. In contrast, in the SCM, the density keeps decreasing as mass disappears while the volume of the char particle remains constant.

Figure 13 shows the profile of ϵ_{sa} along the gasifier length. As slag builds up on the char particle, ϵ_{sa} keeps increasing. However, it should be noted that it does not reach a value of unity since the volume of the unreacted char particle is finite at the end of the gasifier.

Key results from slag detachment scenario

In this work, three discrete detachment diameters, 5, 10 and 15 μm , are considered for the slag droplets. Figure 14 shows the ϵ_{sa} profile along the gasifier. Unlike the complete coalescence scenario, where ϵ_{sa} keeps increasing monotonically, Figure 14 shows a sawtooth-type profile.

As expected, Figure 14 shows that the smaller the detachment diameter, the smaller is the build-up on the char particle's surface. The peaks begin to increase in height along the gasifier because the volume of the char particle shrinks as the char particle reacts. Therefore even though the detachment diameter remains the same for each case, the volume fraction of the slag droplet in comparison to char particle keeps increasing. It should be noted that in real life, it would be expected that the detachment diameter would change along the gasifier. The present study provides an idea of the expected range of variation for that case.

Figure 15 shows profile of ϵ_{sd} , the volume fraction of the detached slag in the bulk of the gasifier. Even though the source term is a discontinuous variable, the profile of ϵ_{sd} is reasonably smooth, especially for smaller detachment diameters.

Figure 16 shows the profile of p_{sl} , i.e., number of slag droplets separated per unit volume per unit time for different slag detachment diameters. As expected, the smaller the detachment diameter, higher the value of p_{sl} . It can be seen that the number density of the slag droplets as well as their sizes significantly impacts the deposition flux to the gasifier wall.

Conclusion

In this work, a HSCSP model of the entrained-flow gasifier has been developed. In this model, the shrinking core model is applied in the initial region of the gasifier while a novel shrinking particle model is developed for the later region. This model is more physically realistic than the traditional SCM, yet yields similar results. The SPM is developed by integrating a continuous model with a particle model. Carbon conversion and gasifier exit conditions obtained from the HSCSP model compare well with the industrial data. The model provides information about the particle density of char particles, fraction of slag droplets that are attached to the char particles, and fraction of slag droplets that are detached but exist in the bulk. In addition, the sizes of char particles and attached slag droplets can be tracked along the gasifier. It is also observed that even though the slag detachment is a discontinuous phenomenon, the profile of the volume fraction of detached slag remains reasonably smooth. The number of slag droplets separated per unit volume per unit time is found to increase considerably as the detachment diameter decreases. This information is very valuable for calculating the slag deposition rate on the gasifier wall. It should be noted that the thickness of the slag layer depends on the slag deposition rate on the gasifier wall and the slag layer thickness is a critical variable to ensure uninterrupted operation of the slagging gasifiers. These aspects will be investigated in our future works.

Notation

A_R = inner cross section area (cm^2)

C_D = drag coefficient

C_p = specific heat (cal/g.k)

d = particle diameter (cm)

D_i = inner gasifier diameter (cm)

e = emissivity

F = view factor

f_s = drag force on solids per unit volume of particles (N/cm^3)

g = acceleration due to gravity (cm/s^2)

H = enthalpy (cal/g)

h = heat transfer coefficient ($\text{cal/cm}^2.\text{k.s}$)

$K_{overall}$ = overall reaction constant ($\text{g/cm}^2.\text{atm.s}$)

k = ash layer or diffusion or surface reaction constant ($\text{g/cm}^2.\text{atm.s}$)

M = mass of particle or droplet (g)

m = mass flow rate (g/s)

N_{ch} = number density of char particles (no. /cm^3)

p_{sl} = number of slag droplets formed per volume per time ($\text{no./cm}^3.\text{s}$)

P_t = pressure (atm)

q = heat ($\text{cal/cm}^2.\text{s}$)

Re = Reynolds number

r_j = reaction rate ($\text{g/cm}^3.\text{s}$)

t = time (s)

T = temperature (k)

U = velocity (cm/s)

V_{cd} = volume of particle or droplet (cm^3)

ω_{ash} = ratio of carbon to ash content in char particle

w_{sl} = number of slag droplets detaching in a control volume ($\text{no./cm}^3 \cdot \text{s}$)

X = solid component

x = axial distance (cm)

γ = ratio of unreacted core to char particle size

y = gas component

Greek letters

ε = void fraction

Δ = change

ρ = density (g/cm^3)

σ = Stefan - Boltzmann constant ($\text{cal/cm}^2 \cdot \text{s} \cdot \text{k}^4$)

τ = residence time (sec)

Γ = rate of char consumption ($\text{g/cm}^3 \cdot \text{s}$)

Subscripts

ash = ash layer

avg = average

cd = critical size

ch = char particle

cond = conduction

conv = convection

diff = diffusion

g = gas

mg = recirculation mass added

rad = radiation

recir = recirculation

rg = recirculation mass removed

rxn = reaction

s = solid

sa = slag attached

sd = slag detached

slag = slag droplet

slag dep = slag deposition

sr = slag remaining

w = wall

skin = outside wall of gasifier

Acronyms

CFD = computational fluid dynamics

HSCSP = hybrid shrinking core shrinking particle

IGCC = integrated gasification combined cycle

PM = particulate matter

RSC = radiant syngas cooler

SCM = shrinking core model

Accepted Article

Literature cited:

- 1) Maustad O. An overview of coal based integrated gasification combined cycle (IGCC) Technology. Publication No. LFEE 2005-002 W;2005, <http://lfee.mit.edu/publications>
- 2) Bennett JP, Kwong K. Failure mechanisms in high chrome oxide gasifier refractories. *Metallurgical and Materials Transactions*. 2011;42A:888-904.
- 3) Williford RE, Johnson KI, Sundaram SK, Pilli S. Effective diffusivity and spalling models for slagging coal gasifiers. *J Am Ceram Soc*. 2008;91(12):4016-4022.
- 4) Clayton SJ, Siegel GJ, Wimer JG. Gasification technologies, gasification markets and technologies - present and future, an industry perspective. US Department of Energy. 2002; DOE/FE-0447.
- 5) Seggiani M. Modelling and simulation of time varying slag flow in a Prenflo entrained-flow gasifier. *Fuel*.1998;77(14):1611-1621.
- 6) Lee HH, Lee JC, Joo YJ, Lee CH. Dynamic modeling of Shell entrained flow gasifier in an integrated gasification combined cycle process. *Applied Energy*. 2014;131:421-440.
- 7) Pilli SP, Johnson KI, Williford RE, Sundaram SK, Korolev VN, Crum JV. Modeling slag penetration and refractory degradation using the finite element method. The Twenty-Fifth Annual International Pittsburgh Coal Conference, September 29 - October 2, Pittsburgh, PA, 2008.
- 8) Bockelie MJ, Denison MK, Chen Z, Linjewile T, Senior CL, Sarofim AF. CFD modeling for entrained flow gasifiers in Vision 21 systems. Proceedings of the 19th Annual International Pittsburgh Coal Conference. September 24–26, Pittsburgh, PA, 2002.
- 9) Benyon PJ. Computational modeling of entrained flow slagging gasifiers. PhD thesis, University of Sydney. 2002. Australia.
- 10) Kasule JS, Turton R, Bhattacharyya D, Zitney SE. Mathematical modeling of a single-stage, downward-firing, entrained-flow gasifier. *Ind. and Eng. Chem. Research*. 2012;51(18):6429-6440.

- 11) Shah J, Govind R. Modeling and simulation of an entrained flow coal gasifier. *AIChE J.* 1984;30(1):79-92.
- 12) Srinivasachar S, Senior CL, Helble JJ, Moore JW. A fundamental approach to the prediction of coal ash deposit formation in combustion systems. *Symposium (International) on Combustion.* 1992;24(1):1179-1187.
- 13) Quann RJ, Sarofim AF. A scanning electron microscopy study of the transformations of organically bound metals during lignite combustion. *Fuel.* 1986;65:40-46.
- 14) Liang Q, Guo X, Dai Z, Liu H, Gong X. An investigation on the heat transfer behavior and slag deposition of membrane wall in pilot scale entrained flow gasifier. *Fuel.* 2012;102:491-498.
- 15) Seames WS. An initial study of the fine fragmentation fly ash mode generated during pulverized coal combustion. *Fuel Processing Tech.* 2003;81:109-125.
- 16) Loehden D, Walsh PM, Sayre AN, Beer JM, Sarofim AF. Generation and deposition of fly ash in the combustion of pulverized coal. *J Institute of Energy.* 1989;451:119-127.
- 17) Yan L, Gupta RP, Wall TF. A mathematical model of ash formation during pulverized coal combustion. *Fuel.* 2002; 81: 337-344.
- 18) Wang P, Massoudi M. Slag behavior in Gasifiers. Part I: Influence of coal properties and gasification conditions. *Energies.* 2013;6:784-806.
- 19) Vaysman V, Lu Y. Quality guidelines for energy system studies. Detailed coal specifications. DOE/NETL-401/012111, 2012.
- 20) Stalder AF, Melchior T, Muller M, Sage D, Blu T, Unser M. Low-Bond Axisymmetric drop shape analysis for surface tension and contact angle measurements of sessile drops. *Colloids and surfaces A: Physicochemical and Engineering Aspects.* 2010;364:72-81.
- 21) Mehta AS, Sahajwalla, V. Influence of temperature on the wettability at the slag/carbon interface during pulverised coal injection in a blast furnace. *Scandinavian Journal of Metallurgy.* 2001;30:370-378.

- 22) Li S, Whitty KJ. Physical phenomena of char–slag transition in pulverized coal gasification. *Fuel Processing Technology*. 2012;95:127-136.
- 23) Li S, Wu Y, Kevill W. Ash deposition behavior during char-slag transition under simulated gasification conditions. *Energy & Fuels*. 2010;24(3):1868-1876.
- 24) Buhre BJP, Hinkley JT, Gupta RP, Nelson PF, Wall TF. Fine ash formation during combustion of pulverised coal-coal property impacts. *Fuel*. 2006;18(2):185-193.
- 25) Maloney D, Monazam K, Casleton KH, Shaddix CR. Evaluation of char combustion models: measurement and analysis of variability in char particle size and density. *Proceedings of the Combustion Institute*. 2005;30:2197-2204.
- 26) Kang SG, Kerstein AR, Helble JJ, Sarofim AF. Simulation of residual ash formation during pulverized coal combustion bimodal ash particle size distribution. *Aerosol Science and Technology*. 1990;13:401-412.
- 27) Helble JJ, Srinivasachar, Boni AA. Factors influencing the transformation of minerals during pulverized coal combustion. *Progress in Energy and Combustion Sciences*. 1990;16:267-279.
- 28) Yu D, Xu MH, Liu X, Huang J, Li G. Mechanisms of submicron and residual ash particle formation during pulverised coal combustion: A comprehensive review. *Developments in Chemical Engineering and Mineral Processing*. 2005;13(3-4):467-482.
- 29) Zhang L. Characterization of Combustion-Derived individual fine particulates by computer controlled scanning electron microscopy. *AIChE*. 2009;55(11):3005-3016.
- 30) Slezak, A, Kuhlman MJ, Shadle JL, Shi S. CFD simulation of entrained-flow gasification: Coal particle density/size fraction effects. *Powder Technology*. 2010;203:98–108.
- 31) Kasule JS, Turton R, Bhattacharyya D, Zitney, SE. One-dimensional dynamic modeling of a single-stage downward-firing entrained-flow coal gasifier. *Energy & Fuels*. 2014;28(8):4949-4957.

- 32) Kumar M, Ghoniem AF. Multiphysics simulations of entrained flow gasification. Part 1: Validating nonreacting flow solver and particle turbulent dispersion model. *Energy and Fuels*. 2012;46:451-463.
- 33) Arastoopour H, Gidaspow D. Vertical pneumatic conveying using four hydrodynamic models. *Ind. Eng. Chem. Fund.* 1979;18(2):123-130.
- 34) Rowe PN, Henwood GA. Drag forces in hydraulic model of fluidized bed. *Trans. Chem. Eng.* 1961;39:43-54.
- 35) Niessen WR. Combustion and incineration processes, 3rd ed. Basel, NY: CRC Press, 2010.
- 36) Fulton CH. Principles of Metallurgy. Norwood, MA: Plimpton Press, 1910.
- 37) Rao RM, Bhattacharyya D, Rengaswamy R, Choudhury, R. S. A two-dimensional steady state model including the effect of liquid water for a PEM fuel cell cathode. *J. Power Sources*. 2007; 173:375-393.
- 38) Syamlal M, Bissett LA. METC Gasifier Advanced Simulation (MGAS) Model; Technical Note. 1992; NITS report No: DOE/METC-92/ 4108 (DE92001111)
- 39) Wen CY, Chaung TZ. Entrainment coal gasification modeling. *Ind. Eng. Chem. Process Des. Dev.* 1979; 18(4): 684-695.
- 40) Aspen Custom Modeler, AspenTech; <http://www.aspentech.com/>.
- 41) Tampa Electric POLK Power Station Integrated Gasification Combined Cycle Project, Final Technical report; Tampa Electric Company; Tampa, FL., 2002. <http://www.netl.doe.gov/technologies/coalpower/cctc/cctdp/bibliography>

List of Figures

Figure 1. Slag formation and detachment.

Figure 2. Hybrid shrinking core shrinking particle (HSCSP) model.

Figure 3. Schematic of solid phase consisting separated slag, attached slag, and char particle.

Figure 4: Schematic of the recirculation model.

Figure 5. Continuum phase domain for solid and gas integrated with the particle phase domain.

Figure 6. Schematic for the slag droplet formation and detachment model.

Figure 7. Schematic of information exchange between the continuum model and particle model.

Figure 8. Comparisons of the mole fractions of CO₂, CO, H₂ and H₂O (on dry basis) at the exit of the RSC with TECO data.

Figure 9. Comparison of the reaction rates between the shrinking particle model and hybrid shrinking core-shrinking particle model.

Figure 10. Comparison of carbon conversion of carbon between the gasifier model and the complete coalescence model.

Figure 11. Comparison of solids temperature profiles between the shrinking core and HSCSP model.

Figure 12. Variation of diameter of char particles, attached slag droplets, and average density of the char-slag system along the gasifier.

Figure 13. Variation of ϵ_{sa} along the gasifier for complete coalescence case.

Figure 14. Variation of ϵ_{sa} along the gasifier for the slag detachment scenario.

Figure 15. Variation of detached slag volume fraction along the gasifier.

Figure 16. Variation of p_{sl} along the gasifier for 10 and 15 micron case.

Table 1. Model parameters and input conditions

Parameters/Conditions	Value
<u>Gasifier parameters</u>	
Length (cm)	662
Internal diameter (cm)	179
<u>Operating conditions</u>	
Coal slurry flow rate (g/s)	61232.9
Particle diameter (μm)	100
Water to coal ratio	0.4115
O ₂ to coal ratio	0.8347
Inlet Temperature ($^{\circ}\text{C}$)	29.85
Inlet Pressure (bar)	28.33

Table 2. Proximate and Ultimate analysis of Illinois #6 coal

Illinois #6	As-Received (wt %)
<u>Proximate analysis</u>	
Fixed Carbon	44.19
Ash	9.99
Volatile matter	34.70
Moisture	11.12
<u>Ultimate analysis (DAF)</u>	
C	63.75
H	4.50
O	6.88
N	1.25
S	2.51

Accepted Article

Table 3. Validation data from TECO power plant⁴⁰

Conditions	TECO
Gasifier configuration³⁰	
Internal diameter (cm)	179
Length (cm)	662
Operating conditions	
Coal feed rate (kg/s)	40
Coal particle size (μm)	100
Oxygen/coal ratio	0.82806
Water/coal ratio	0.4108
Pressure (atm)	26

Accepted Article

Table 4. Comparison between outlet mole fractions of SCM and HSCSP models.

Component	SCM	HSCSPM
CO ₂	0.22396	0.22531
CO	0.47236	0.47052
H ₂	0.01848	0.01842
H ₂ O	0.20823	0.20883

Accepted Article

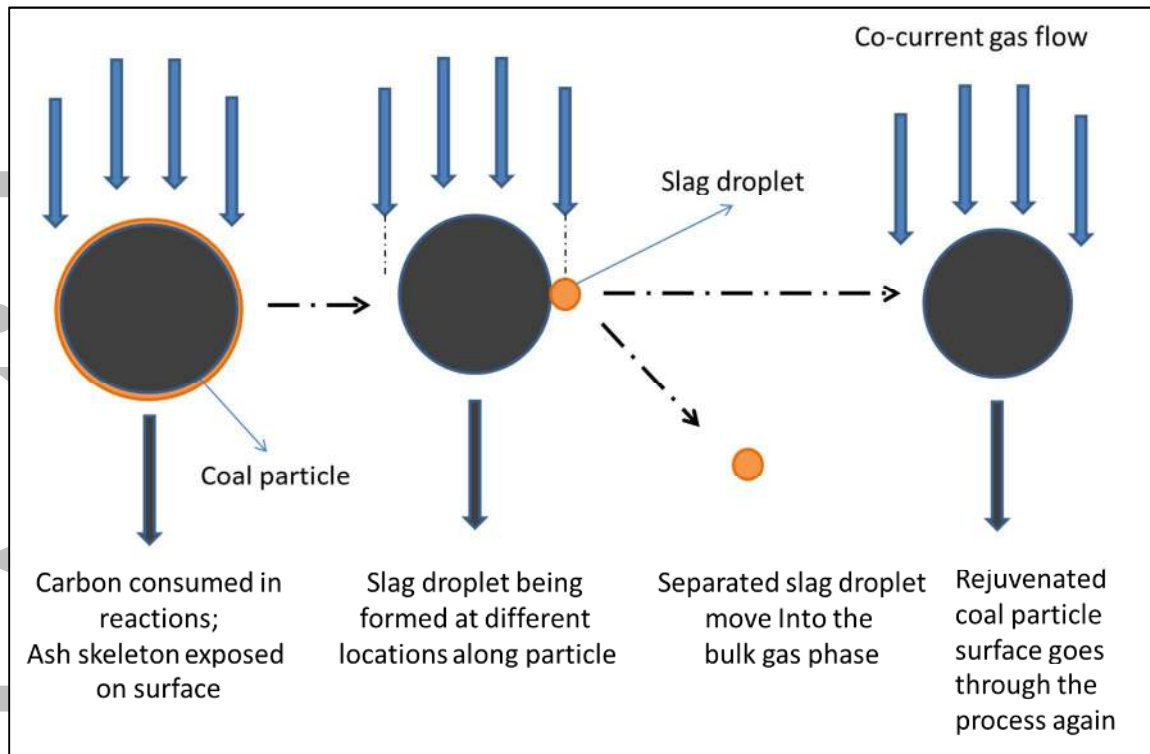


Figure 1. Slag formation and detachment.

Accepted

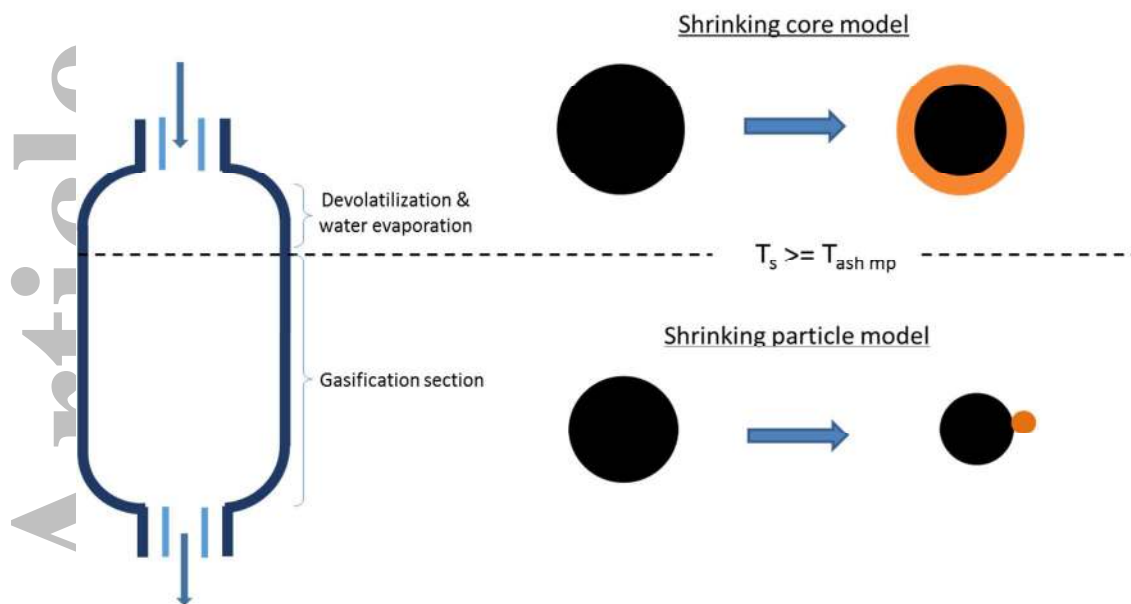


Figure 2. Hybrid shrinking core shrinking particle (HSCSP) model.

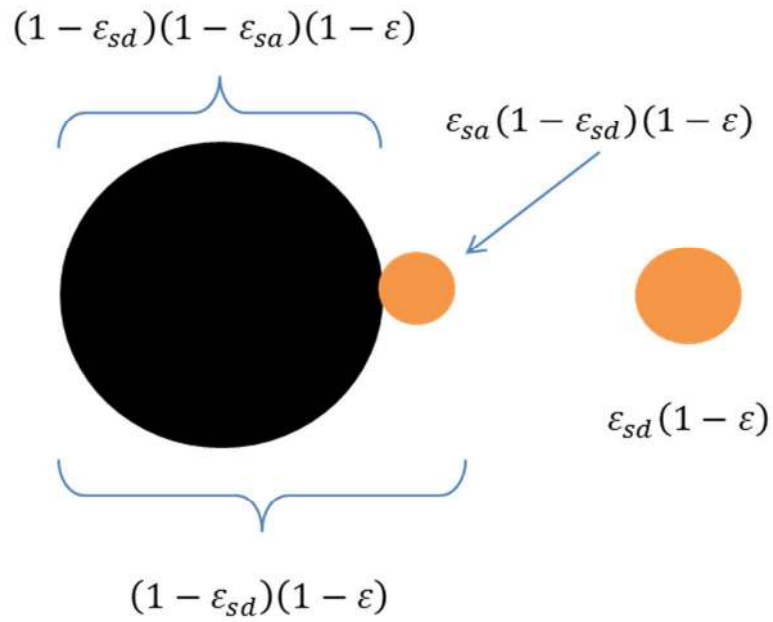


Figure 3. Schematic of solid phase consisting separated slag, attached slag, and char particle.

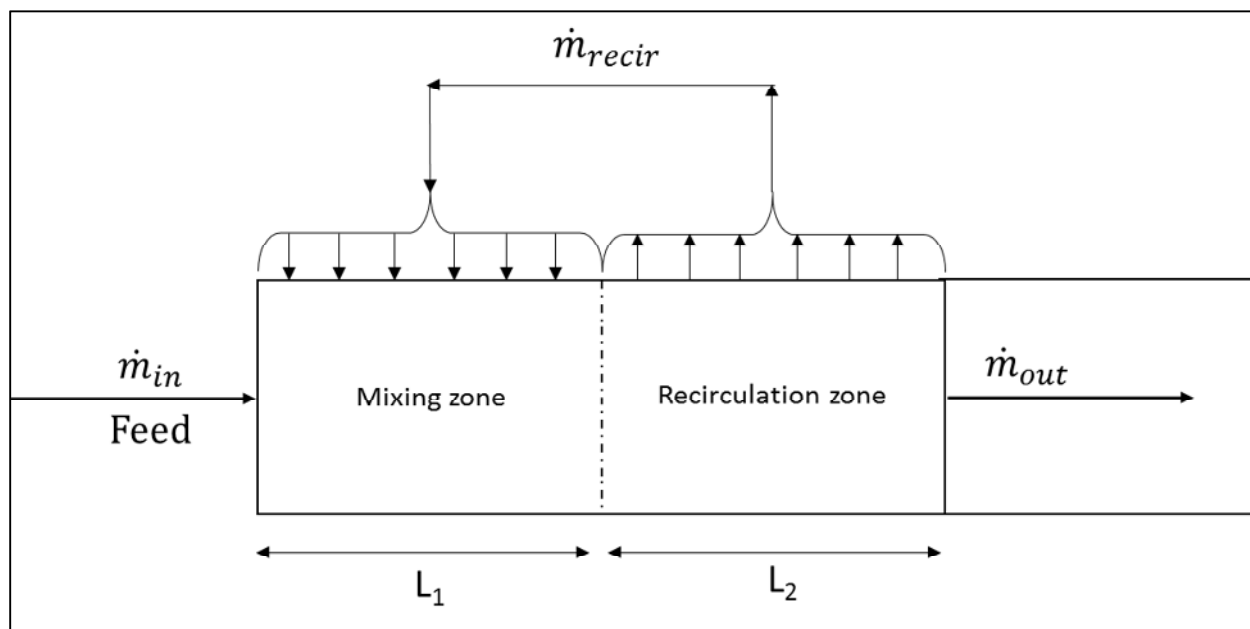


Figure 4. Schematic of the recirculation model.

Accepted

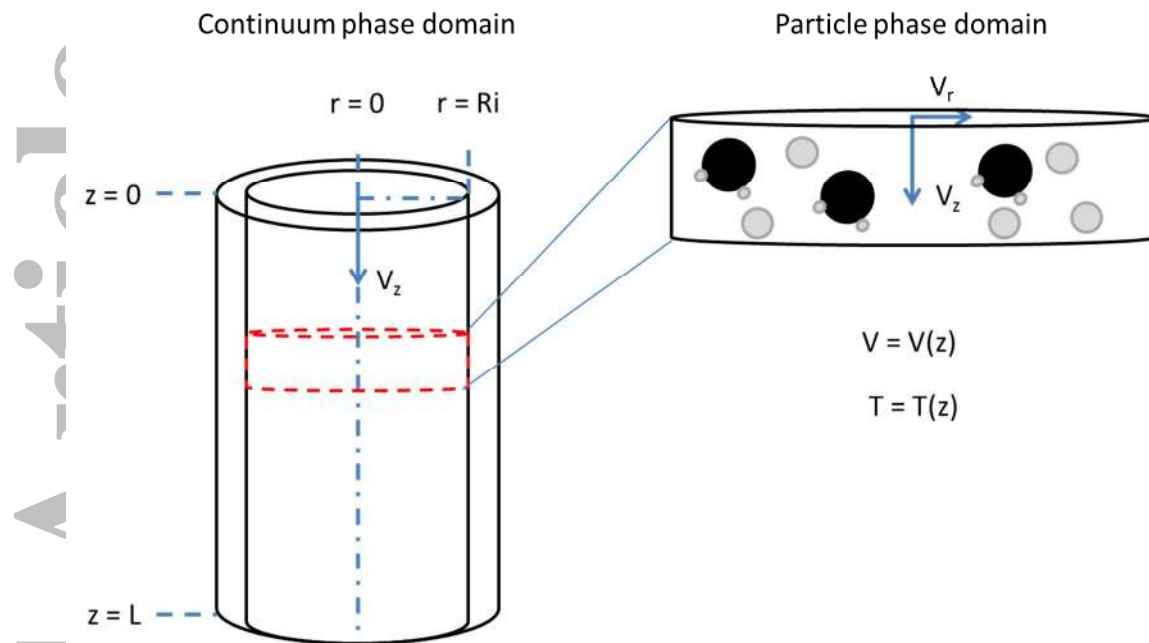


Figure 5. Continuum phase domain for solid and gas integrated with the particle phase domain.

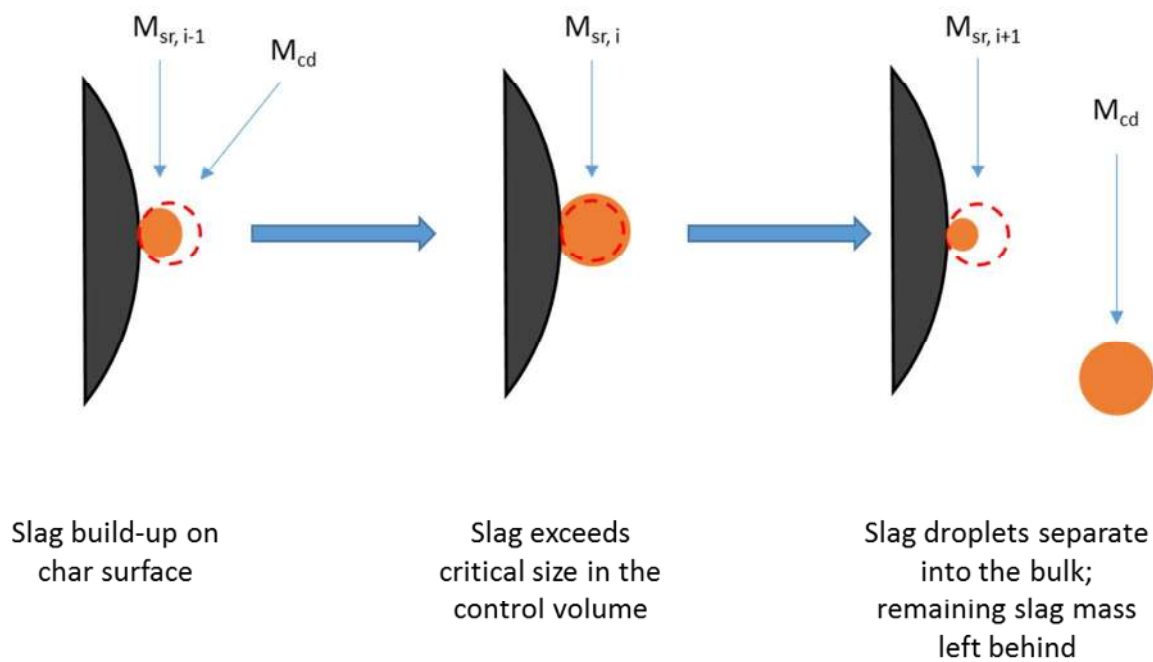


Figure 6. Schematic for the slag droplet formation and detachment model.

Accepted

Accepted Article

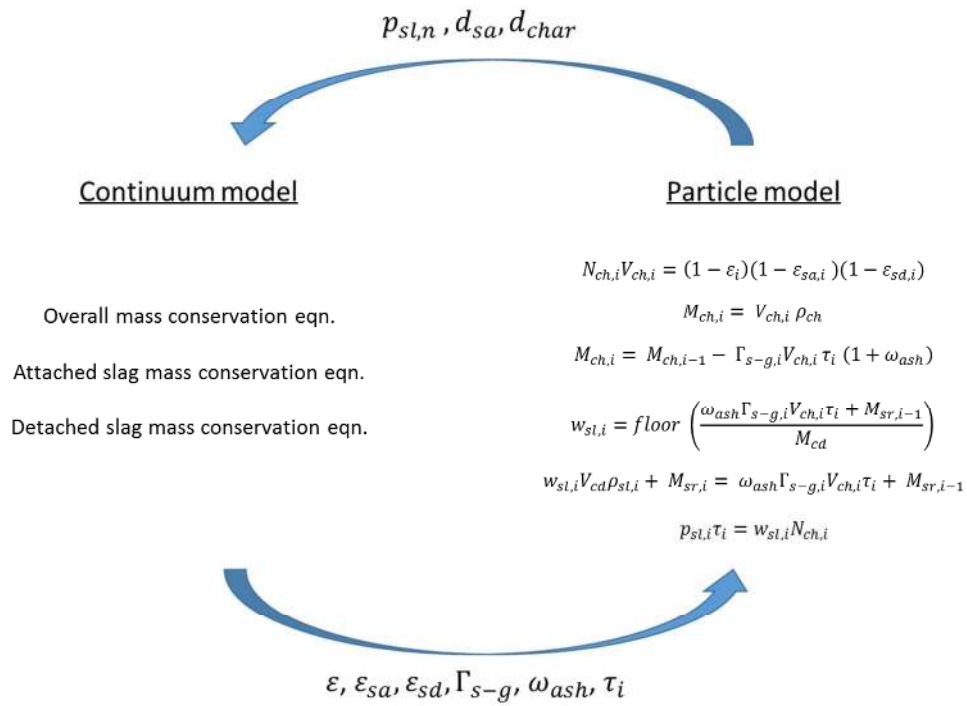


Figure 7. Schematic of information exchange between the continuum model and particle model.

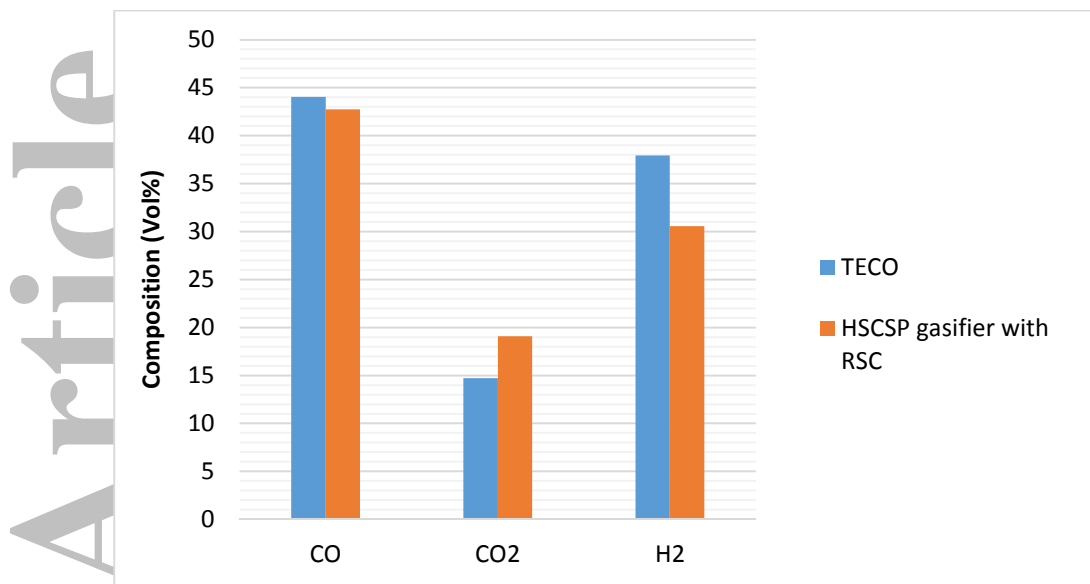


Figure 8. Comparisons of the mole fractions of CO₂, CO, H₂ and H₂O (on dry basis) at the exit of the RSC with TECO data.

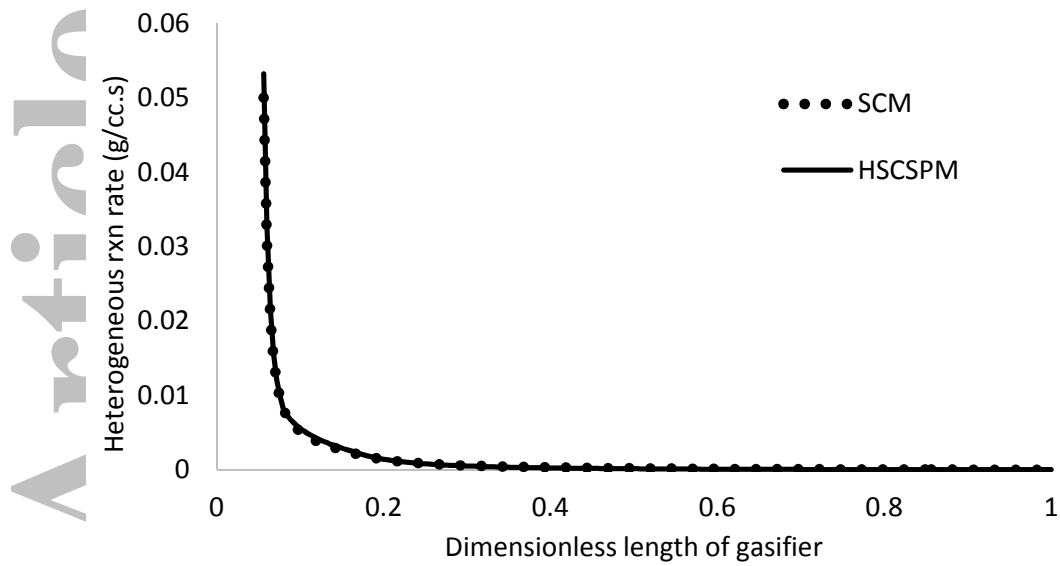


Figure 9. Comparison of the reaction rates between the shrinking particle model and hybrid shrinking core-shrinking particle model.

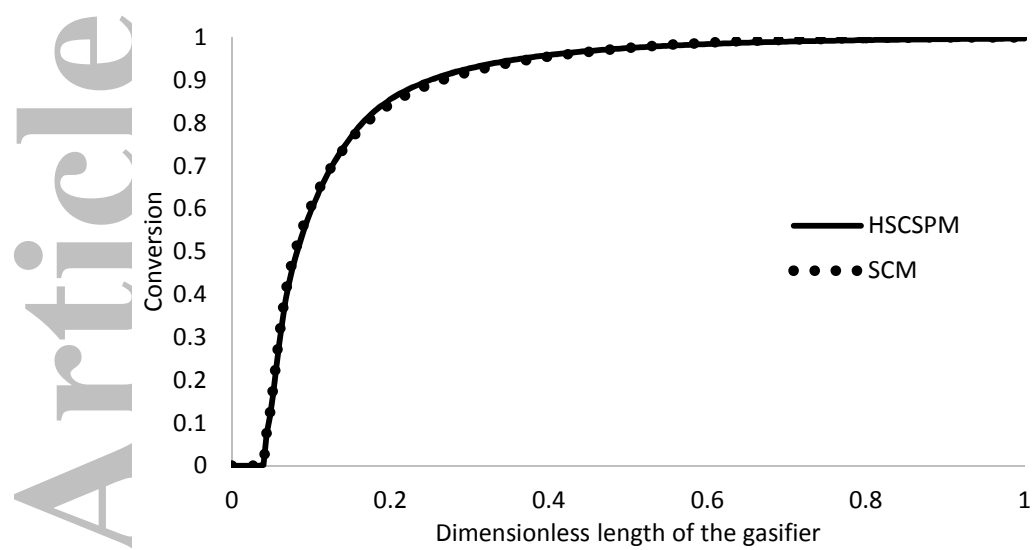


Figure 10. Comparison of carbon conversion of carbon between the gasifier model and the complete coalescence model.

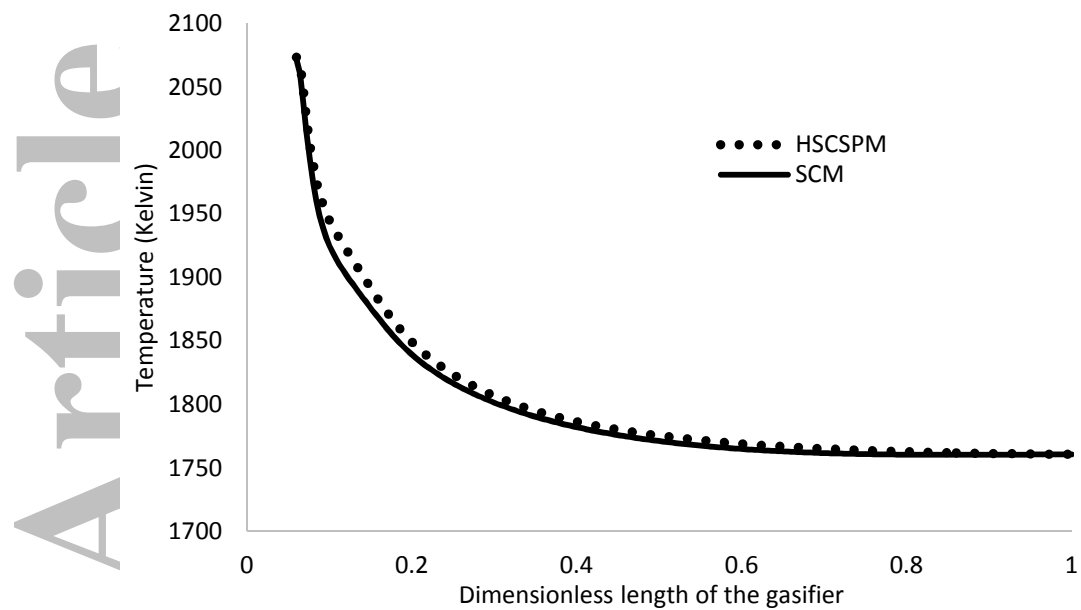


Figure 11. Comparison of solids temperature profiles between the shrinking core and HSCSP model.

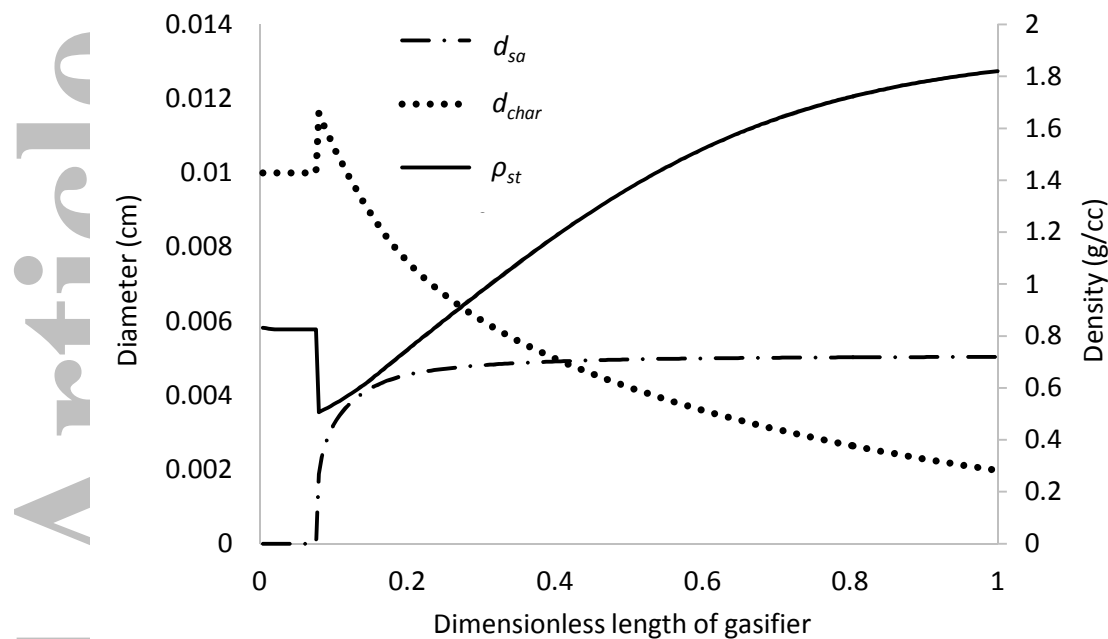


Figure 12. Variation of diameter of char particles, attached slag droplets, and average density of the char-slag system along the gasifier.

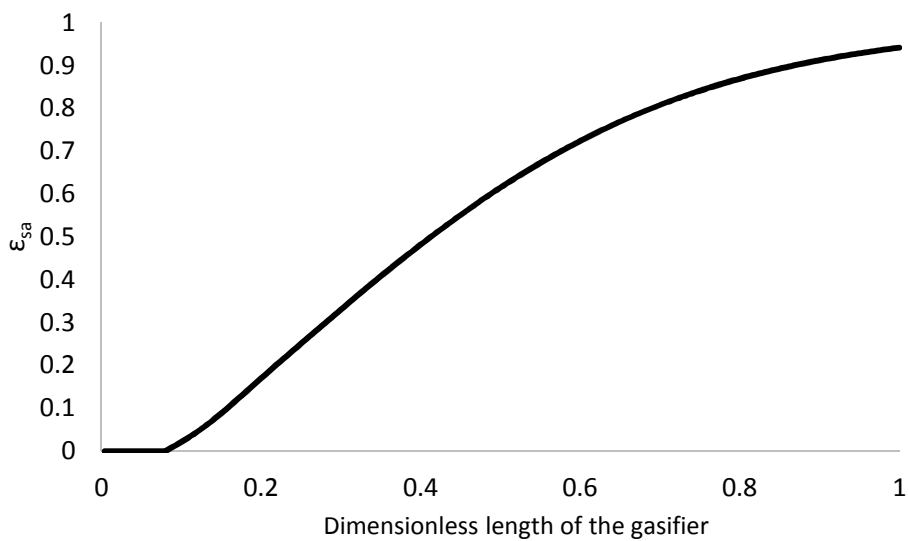


Figure 13. Variation of ϵ_{sa} along the gasifier for complete coalescence case.

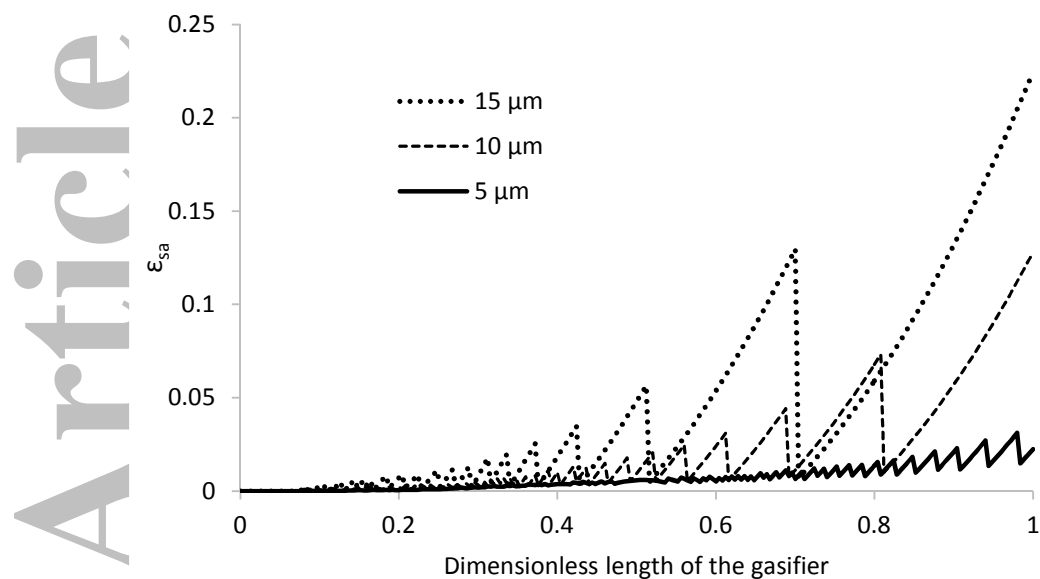


Figure 14. Variation of ϵ_{sa} along the gasifier for the slag detachment scenario.

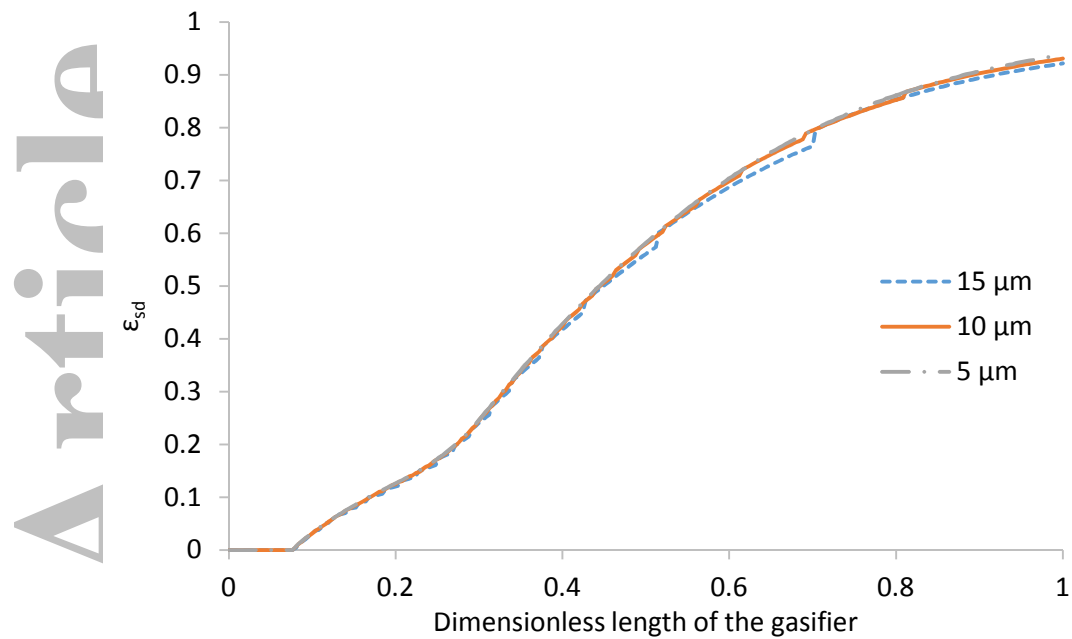


Figure 15. Variation of detached slag volume fraction along the gasifier.

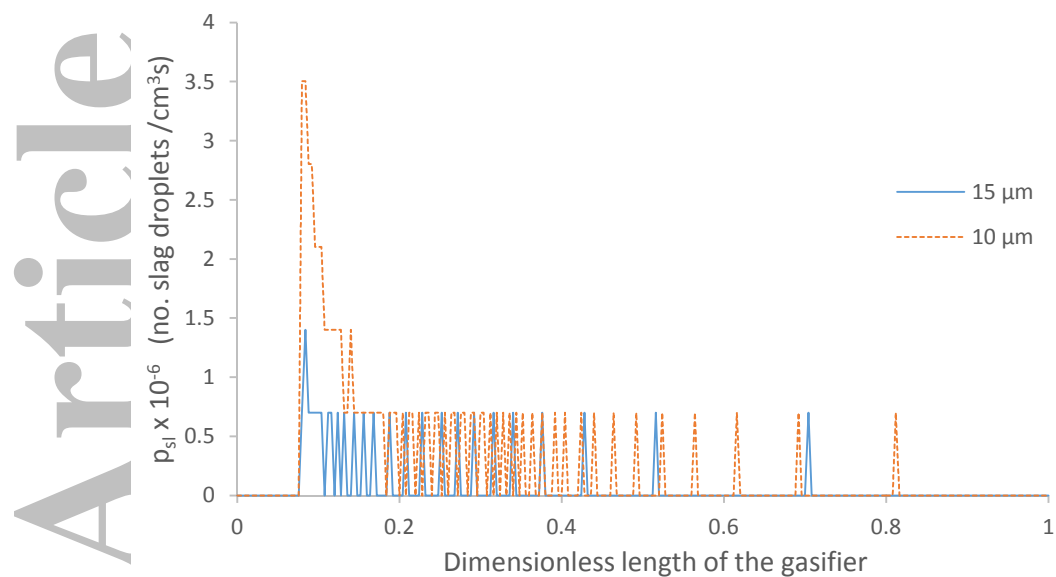


Figure 16. Variation of p_{sl} along the gasifier for 10 and 15 micron case.